symmetry

MDPI

Article

Hyperbolic Electromagnetism and Metrological Closure of Vacuum Impedance with Links to Topological Response in Metals and Alloys

Tihomir Car

Rudjer Bošković Institute, Bijenička Cesta 54, 10000 Zagreb, Croatia; car@irb.hr

Abstract

We develop a symmetry-based reconstruction of the vacuum impedance and the fine-structure constant. Hyperbolic geometry and discrete sectorization of the electromagnetic field plane are the only input assumptions. The construction identifies a unique integer-square hyperbolic selector that fixes the electric–magnetic partition without adjustable parameters. This yields the geometric part of the vacuum impedance when combined with the quantum scale h/e^2. The same discrete structure provides a normalization for the fine-structure constant through a universal sector angle $\pi/24$. We discuss how discrete rotational and modular symmetries, commonly realized in crystalline metals and layered heterostructures, provide experimentally accessible settings to probe the proposed geometric structure through electromagnetic and transport measurements.

Keywords: hyperbolic geometry; electromagnetic duality; topological quantization; modular structure; functional materials

1. Introduction

Symmetry and topology play a central role in modern physics. We find them from the classification of phases of matter to the quantization of response coefficients in condensed-matter and field theoretic systems. Quantities such as the quantum Hall conductance, the topological polarization angle, and the magnetoelectric response of topological insulators derive their robustness from discrete geometric structures and symmetry-protected invariants [1–4].

Electromagnetism exhibits an analogous internal structure. The Maxwell equations possess a continuous duality symmetry. They mix electric and magnetic fields, which becomes discrete in the presence of quantized charge [5,6]. In geometric formulations, this duality is naturally captured by the action of modular transformations on a complex field variable, linking electromagnetic response parameters to hyperbolic geometry and invariant forms [7]. These structures underlie the quantization of the Hall conductance and the von Klitzing constant $R_K = h/e^2$ [8]. Also, more generally, they underlie the appearance of universal dimensionless numbers in gauge theories.

The impedance of free space, $Z_0 = \sqrt{\mu_0/\varepsilon_0}$, is traditionally treated as a fixed electromagnetic constant. However, the 2019 redefinition of SI units, which placed Planck's constant h and the elementary charge e as exact reference values, shifted the hierarchy: μ_0 and ε_0 are now derived from (h, e, α, c) rather than fundamental inputs [9]. This shift raises the question of whether the value of Z_0 reflects a deeper geometric or symmetry-driven structure.

Academic Editors: Vasilis K. Oikonomou and Zine El Abiddine Fellah

Received: 17 December 2025
Revised: 22 January 2026
Accepted: 28 January 2026
Published: 2 February 2026

An additional motivation comes from the topological quantization of electromagnetic response coefficients. In topological materials, the electromagnetic θ–term links bulk topology to boundary response, producing fractionalized or quantized values of optical and transport coefficients. An example is the topological magnetoelectric effect, where the fine-structure constant (α_{EM}) itself appears as a quantized coefficient in the effective action [10]. In this framework, α_{EM} acquires the status of a topological angle. Its value reflects discrete geometric or symmetry constraints. Closely related developments include the quantization of optical rotation, axion electrodynamics, and the emergence of universal EM responses protected by time-reversal or inversion symmetry in insulating phases [11–13]. These results suggest that electromagnetic constants traditionally viewed as fixed parameters of the vacuum may in fact encode deeper geometric or topological structures. This is an idea that is strongly coupled with the symmetry-based construction developed here.

Several well-established phenomena in solid-state physics illustrate how dimensionless geometric phases govern electromagnetic responses in metallic systems. Flux quantization in superconducting metallic loops arises from the single-valuedness of the condensate wavefunction, yielding the universal quantum $\Phi_0 = h/(2e)$ [14–16]. Berry and Zak phases appear naturally in metals and alloys with nontrivial band topology, where electronic states acquire geometric phases over Brillouin-zone loops, influencing polarization, orbital magnetism, and transport [4,17–19]. Quantized Hall conductance in two-dimensional electron systems and in topological metallic films is governed by integer Chern numbers, producing the universal plateaus $\sigma_{xy} = \nu e^2/h$ independent of microscopic material details [1,2,8,20]. These examples demonstrate that dimensionless geometric and topological invariants, such as Berry phases, winding numbers, and Chern integers, play a central role in determining electromagnetic responses across a wide class of metallic and alloyed systems. Also, crystalline and quasi-crystalline metals exhibit discrete rotational symmetries (C_6, C_{12}) and reciprocal-space sectorization that directly mirror the modular structure used in our geometric construction [21].

In this work we propose a geometric reconstruction of the vacuum impedance based on Lorentz-invariant hyperbolic geometry and its natural discrete sectorization. We show that the complex field-plane representation used in duality-symmetric electromagnetism admits a unique hyperbolic selector. This fixes the relative weighting of the electric and magnetic channels through the integer-square pair $(6, 5)$. This selector acts analogously to a topological invariant: it is fixed by hyperbolic symmetry, does not rely on dynamical assumptions, and determines a unique geometric factor that multiplies the universal metrological scale h/e^2.

We also show that the same geometric structure provides a natural normalization for the fine-structure constant α_{EM}, linking it to a discrete angle $\pi/24$ associated with sectorization of the (E, B) plane. This interpretation mirrors familiar constructions in topological phases of matter, where Berry phases, Chern numbers, and polarization angles encode geometric information about the underlying Hilbert-space bundle. Taken together, these results place the vacuum impedance and electromagnetic coupling constants within a unified symmetry-geometric framework. Because the geometric selector and the sector angle $\pi/24$ contain no adjustable parameters, the resulting expressions for Z_0 and α_{EM} are experimentally falsifiable.

2. Geometric and Physical Framework

A central structural feature of electromagnetism is that the electric charge appears as a holonomy of the underlying $U(1)$ connection. In differential-geometric language, the gauge potential A_μ defines a principal $U(1)$ bundle over space–time, and the quantization of electric charge is equivalent to the quantization of the associated holonomy around non-

contractible loops. This viewpoint, standard in gauge theory and condensed-matter physics, underlies Dirac's argument for charge quantization, the Aharonov–Bohm effect, and the geometric interpretation of Berry phases and polarization in solids [22–24]. In the present framework we retain only these minimal and conventional parts. Electric charge sets a dimensionless phase scale, while the metrological constant h/e^2 supplies the physical unit. No additional assumptions about the microscopic origin of charge are needed for the geometric reconstruction developed below.

In standard $U(1)$ gauge theory, the electric charge q enters only through the phase factor $e^{iq\theta}$ acting on matter fields. The value of q is not fixed by the gauge symmetry itself. The $U(1)$ does not quantize charge, and in the absence of additional topological structures (such as monopoles or nontrivial bundles), q may take any real value. What is fixed is the fact that charge appears solely as a generator of a dimensionless phase. This observation is crucial for the present construction. If the physical role of charge is to generate a phase, then all dimensionless electromagnetic response coefficients must ultimately be expressible in terms of phase ratios. In particular, any decomposition of the electromagnetic field into "electric" and "magnetic" channels should be describable by a complex phase vector.

In solid-state systems, the quantization of flux, polarization, and Hall conductance arises from winding numbers of Berry connections, independent of microscopic units [4,17,18]. From this viewpoint, the dimensional content of electric charge in the SI is not fundamental but imposed by metrological convention. The underlying "topological charge" is a phase quantity without intrinsic units.

Hyperbolic geometry provides the natural Lorentz-invariant arena in which such dimensionless charges can be embedded. The Minkowski metric selects the quadratic form

$$B^2 - E^2 = 1, \tag{1}$$

as the unique invariant under changes of inertial frame. Any split of the electromagnetic degrees of freedom into "electric" and "magnetic" channels must therefore lie on a branch of the unit hyperbola. In a dynamical-systems sense, such points are hyperbolic fixed points. Their linear stability matrix has purely real eigenvalues, with no center manifold and therefore no rotational ambiguity [25]. This structural stability makes hyperbolic points excellent geometric selectors.

To connect a continuous Lorentz-invariant constraint with symmetry-protected responses in condensed matter, we impose a discretization hypothesis: the physically distinguishable channel partitions correspond to a discrete subset of the continuous hyperbola. This is the standard situation whenever a response is protected by a quantized phase or by a quantized transport coefficient. The measurable sectors are labeled by integers, while continuous deformations leave the label unchanged. Therefore, we restrict attention to rational points on the unit hyperbola, $B^2 - E^2 = 1, B^2, E^2 \in \mathbb{Q}$. After clearing a common denominator, it can be represented by integer pairs. This does not claim that the vacuum fields themselves are integer-valued. This only states that the sector labels of a discrete symmetry-protected partition can be taken on a lattice (up to an overall scale).

In this spirit we represent the electromagnetic degrees of freedom by a complex selector $z = B + iE$, which plays the same structural role as the Riemann–Silberstein vector $\mathbf{F} = \mathbf{E} + ic\,\mathbf{B}$ introduced in early complex formulations of Maxwell theory and widely used in modern photonics and field theory [26,27]. In both constructions, the electromagnetic field is encoded into a single complex quantity whose modulus and phase carry invariant information. Our selector differs only by normalization and by the imposition of a hyperbolic constraint $B^2 - E^2 = 1$.

In addition, when the electromagnetic channels are represented on the hyperbola through a complex selector $z = B + iE$, it is natural to require that the Lorentz-invariant

data B^2 and E^2 be integer-valued. This is the discrete remnant of the continuous duality symmetry. In modular formulations of electromagnetism and in topological phases of matter, the electromagnetic coupling space is acted upon by $\mathrm{SL}(2,\mathbb{Z})$ [7], whose invariants select integer quadratic forms. Imposing that (B^2, E^2) lie in this integer lattice forces the hyperbolic constraint $B^2 - E^2 = 1$ to admit only a small number of minimal solutions, i.e., not all integer solutions of Equation (1) are physically admissible.

To obtain a discrete, physically meaningful selector, we require that the coordinates (B^2, E^2) lie in the integers and satisfy minimal and model independent conditions:

1. *Non–degeneracy (both channels active).* Pairs with $E^2 = 1$ are discarded because they represent a trivial "electric" channel and no genuine partitioning of the hyperbola. Thus, $(2, 1)$ is excluded.
2. *Irreducibility (squarefree channels).* The values of B^2 and E^2 must be squarefree integers. This removes hidden quadratic rescalings and ensures that the ratio B^2/E^2 reflects an intrinsic rather than reducible geometric split. Pairs such as $(4, 3)$ are therefore excluded since 4 contains a perfect square.
3. *Hyperbolic discriminant (modular origin).* In duality-symmetric formulations the natural arithmetic invariant of a hyperbolic modular element is its discriminant. For a representative with trace t, the discriminant is $D = t^2 - 4$. The smallest hyperbolic trace is $t = 3$, hence

$$D_{\min} = 3^2 - 4 = 5, \tag{2}$$

so the first nontrivial hyperbolic discriminant is governed by $\sqrt{5}$. We therefore require that the selector engages this minimal non-Euclidean content, i.e., that the electric channel carries the minimal squarefree discriminant $E^2 = 5$. Combined with the unit-gap condition $B^2 - E^2 = 1$, this fixes the minimal admissible integer-square point to $(B^2, E^2) = (6, 5)$ and hence $z = \sqrt{6} + i\sqrt{5}$ (see Figure 1 as an example).

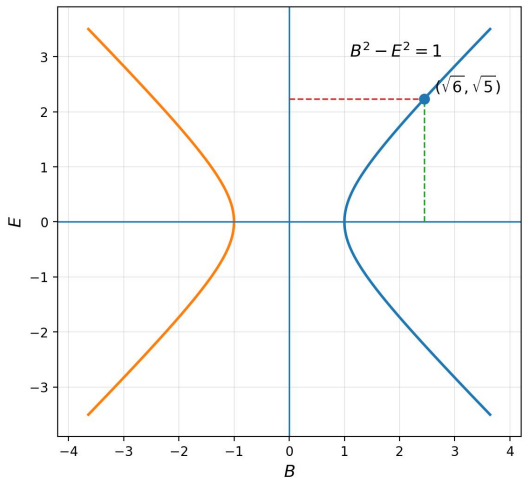

Figure 1. Lorentz-invariant unit hyperbola $B^2 - E^2 = 1$ in the (B, E) plane. The highlighted point $(\sqrt{6}, \sqrt{5})$ is the minimal squarefree hyperbolic selector satisfying the imposed symmetry criteria.

The integer-square hyperbolic sector introduced here should be understood as a minimal and nondegenerate geometric choice. Requiring both electric and magnetic channels to be simultaneously active and free of trivial rescalings uniquely selects the pair $(B^2, E^2) = (6, 5)$. Small perturbations of this choice do not preserve the unit hyperbolic constraint together with discreteness, indicating that the construction is rigid rather than fine-tuned. The role of the quantum scale is purely metrological: it converts the dimensionless geometric factor into a measurable impedance without altering the underlying geometry.

Thus, the Lorentz geometry, the minimality of the hyperbolic discriminant, and the requirement of a nondegenerate partition together single out the complex selector z without adjustable parameters. This selector provides the canonical real-imaginary balance that appears throughout the geometric reconstruction of electromagnetic quantities.

Vacuum Impedance from the Hyperbolic Selector

In classical electrodynamics the free-space impedance is introduced as

$$Z_0 = \sqrt{\mu_0/\varepsilon_0} \approx 120\pi\ \Omega, \tag{3}$$

a property of free space that sets the balance between electric and magnetic fields in a propagating wave. Dimensionally,

$$[Z] = \frac{[h]}{e^2}, \tag{4}$$

so an expression for Z_0 requires a dimensionless geometric factor and a dimensional anchor carrying ohms.

Once the hyperbolic selector is fixed, the only remaining freedom is an overall scale relating the dimensionless (B, E) to physical fields. In conventional electrodynamics the vacuum impedance may be written as $Z_0 = |E|/|H|$, i.e., as the ratio between the electric field amplitude and the magnetic field intensity in a plane wave. In our normalization we factor out the metrological scale h/e^2 and treat Z_0 in geometric units, where it is a pure number that depends only on the relative partition between the electric and magnetic channels.

In any two-channel description of electromagnetism, the physically relevant vacuum response must be built in a rotation invariant scalar constructed from the two channel amplitudes. Given the hyperbolic constraint $B^2 - E^2 = 1$, the remaining independent scalar built from (E, B) that is symmetric under channel exchange up to reciprocity, vanishes if either channel is switched off, and is insensitive to the sign choices is the mixed invariant $(EB)^2$. It is the minimal scalar measuring the simultaneous participation of both channels.

To connect this dimensionless invariant to an isotropic free-space response, we normalize by the unique isotropic solid-angle factor 4π. This is the same normalization that appears whenever a flux or intensity-like quantity is promoted to a rotationally invariant "total" measure on the sphere. Therefore, we define the dimensionless geometric impedance factor as follows:

$$Z_0^{(\mathrm{geom})} = 4\pi(EB)^2. \tag{5}$$

The ohmic dimension is supplied independently by quantum metrology through h/e^2. The present step fixes only the dimensionless geometric factor.

The factor $Z_0^{(\mathrm{geom})}$ in Equation (5) is dimensionless. In SI units, electrical resistance is realized through quantum electrical standards, and the natural scale is the von Klitzing constant

$$R_K = \frac{h}{e^2} \qquad [R_K] = \Omega. \tag{6}$$

We therefore write the physical vacuum impedance as

$$Z_0 \;=\; Z_0^{(\mathrm{geom})} \times \mathcal{C} \times R_K, \tag{7}$$

where $\mathcal{C}$ is a dimensionless conversion factor fixed by the conventional choice of electromagnetic units. In the SI convention this factor is $\mathcal{C} = 2\alpha$, so that $Z_0 = 2\alpha R_K$. In this way, geometry fixes the dimensionless content, while metrology fixes the unit.

Although physically it provides a richer environment, the group PSL(2,Z) is not necessary in this approach. In this construction, it is sufficient to use the group SL(2,Z),

since the modular structure appears only as an arithmetic organization of the hyperbolic space and does not require the identification of matrices that differ in sign.

Figure 2 illustrates how the discrete structure of the electromagnetic field plane naturally encodes a hyperbolic geometry. This will be later connected to topological response functions in condensed-matter systems. The discrete organization of the electromagnetic field plane implies the existence of topologically protected response channels. The electromagnetic response functions are enhanced or localized by geometry rather than by field strength. Such effects are well established experimentally in quantum Hall systems, topological insulators, and Zak-phase-controlled polarization phenomena.

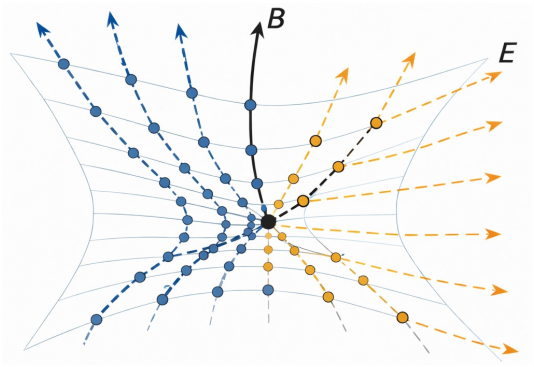

Figure 2. Schematic representation of a discretized electromagnetic field plane. Electric and magnetic field components form orthogonal channels whose discrete organization reflects an underlying hyperbolic geometry.

A closely related geometric–topological structure appears in the bulk–boundary correspondence of topological insulators, where discrete sectors of electromagnetic response are protected by symmetry and topology. As an illustration see for example Figure 1c,f of Ref. [2].

3. Geometric Indication for the Fine-Structure Constant

While our main result concerns the reconstruction of the vacuum impedance, the same hyperbolic geometry also suggests a natural link to the fine-structure constant α_{EM}. Historically, α was first introduced by Sommerfeld in the context of the relativistic correction to the hydrogen spectrum [28] and was later recognized as the universal coupling strength of quantum electrodynamics [29,30]. Despite its central role, the origin of α_{EM} has remained elusive: it is treated as an empirical input in the Standard Model [31].

In our framework, the discrete angle $\pi/24$ arising from sectorization of the (E, B) plane and the hyperbolic seed $z = \sqrt{6} + i\sqrt{5}$ together provide a dimensionless normalization that reproduces the empirical value of α_{EM} to high accuracy. This hints that part of the mystery surrounding α may be geometrical: the constant emerges not from dynamical assumptions, but from the discrete symmetry of hyperbolic geometry underlying the electromagnetic sector.

Therefore, assume the electrodynamic phase degree of freedom admits three operational discretizations with step angles $\pi/6$, $\pi/12$, and $\pi/8$ (e.g., independent phase plates or polarization–phase modulators). Then, the combined interferometric observable obeys the exact identity

$$\frac{\sin(\pi/6) + \sin(\pi/12)}{\sin(\pi/8)} = 2\cos(\pi/24), \tag{8}$$

so that the common sector angle is $\theta_\star = \pi/24$ (LCM$(6, 12, 8) = 24$). With the hyperbolic selector $z = \sqrt{6} + i\sqrt{5}$ (hence $|z|^2 = 11$), the geometric–metrological normalization

$$4\pi\, \alpha_{EM}\, |z|^2 \;=\; \sec\theta_\star \tag{9}$$

predicts

$$\boxed{\alpha_{EM} \;=\; \frac{\sec(\pi/24)}{4\pi\,|z|^2} \;=\; \frac{\sec(\pi/24)}{44\pi}}. \tag{10}$$

Any experimental violation of Equation (8) under clean $\{\pi/6, \pi/12, \pi/8\}$ discretizations falsifies the sectorization hypothesis; conversely, confirmation fixes $\theta_\star$ and tests Equation (9) without invoking μ_0 or ε_0.

It is important to say that no claim is being made here regarding a derivation or reinterpretation of the fine-structure constant. Rather, the appearance of $\pi/24$ is interpreted as a geometric and symmetry-related indicator, suggesting a possible structural coherence between electromagnetic response in condensed matter and more fundamental geometric frameworks.

Operationally, the integers $(6, 12, 8)$ arise here from purely electrodynamic considerations: phase and polarization discretizations at angles $\pi/6, \pi/12, \pi/8$ yield the exact identity (8), fixing the common sector at $\pi/24$. Thus, the photon is the natural carrier of this symmetry. Remarkably, the same triplet also appears in the structure of the Standard Model: six quark flavors, twelve fermionic states per generation, and eight gluons as the generators of $SU(3)_{\text{color}}$ [31,32]. This broader coincidence may suggest that the electromagnetic sector encodes a deeper discrete skeleton on which the full gauge structure is built, though our derivation requires only the photonic degree of freedom.

Now, we can adopt the geometric ansatz for the fine-structure constant which fixes all dimensionless content by the discrete sector angle $\pi/24$ and the hyperbolic selector. The SI-consistent form $Z_0 = 2\,\alpha_{EM}\, h/e^2$ yields

$$\boxed{Z_0 \;=\; \frac{h}{e^2}\,\frac{\sec(\pi/24)}{2\pi\,|z|^2} \;=\; \frac{h}{e^2}\,\frac{\sec(\pi/24)}{22\pi}}. \tag{11}$$

where h/e^2 supplies the ohmic dimension, while the factor $\sec(\pi/24)/(2\pi|z|^2)$ is purely geometric. Numerically, one obtains $Z_0 \approx 376.9\,\Omega$, consistent with the empirical vacuum impedance.

Equation (11) is algebraically equivalent to the well-known metrological form $Z_0 = 2\alpha R_K$, but it makes explicit that all dimensionless content is geometric ($\pi/24$, $|z|^2$), whereas the ohmic unit arises solely from h/e^2.

The various expressions for Z_0 are algebraically equivalent once the fine-structure constant α and the von Klitzing constant $R_K = h/e^2$ [8] are introduced (see Table 1). The SI system treats Z_0 as a derived quantity. Our derivation shows that this form is not only equivalent but also geometrically anchored: the factor 2α emerges from the hyperbolic selector, while the dimensional scale h/e^2 is fixed by quantum metrology.

Table 1. Equivalent forms of the free-space impedance Z_0.

Standard SI (pre-2019)	$Z_0 = \mu_0 c = \sqrt{\mu_0/\varepsilon_0}$
Current SI (post-2019)	$Z_0 \approx 376.730\,\Omega$ (measured, small uncertainty)
Quantum metrology form	$Z_0 = 2\,\alpha\, R_K, \quad R_K = \dfrac{h}{e^2}$
Geometric–metrological form	$Z_0 = 2\,\alpha\,\dfrac{h}{e^2} \;=\; 4\pi\,(EB)^2$

4. Topological α–Quantization in Metals and Alloys

Topological quantization phenomena play a important role in modern metallic and alloy systems. In these materials, quantized electromagnetic responses arise not from energy gaps but from the geometry of Bloch wavefunctions, Berry curvature, and symmetry-protected topological invariants. Several experimentally verified mechanisms realize discrete electromagnetic phases proportional to the fine-structure constant α or its rational multiples. These mechanisms work in much the same way as our hyperbolic selector. They break the geometry into cleanly separated sectors, with $\pi/24$ emerging as the selected angle. This suggest that metals and alloys naturally include the same type of topological behavior.

For example, in magnetic topological materials (like Weyl/Dirac metals), the electromagnetic response acquires an axion term of the form

$$S_\theta = \frac{\alpha}{4\pi^2}\,\theta \int \mathbf{E}\cdot\mathbf{B}\, d^3x\, dt,$$

where the axion angle θ is quantized to 0 or π by time-reversal or inversion symmetries. When $\theta = \pi$, the magnetoelectric response is quantized:

$$\mathbf{P} = \frac{\alpha}{\pi}\,\mathbf{B}, \qquad \mathbf{M} = \frac{\alpha}{\pi}\,\mathbf{E}.$$

This effect has been theoretically predicted [33] and experimentally confirmed in real materials such as $MnBi_2Te_4$ and Mn_3Sn, which are metallic or semimetallic while retaining topologically quantized magnetoelectric couplings [34,35]. Thus, metals can exhibit an electromagnetic response quantized in units of α.

Also, various metallic systems display quantized or fractional anomalous Hall conductivity,

$$\sigma_{xy} = C\,\frac{e^2}{h}, \qquad C \in \mathbb{Q},$$

despite having a Fermi surface. In heavy-fermion alloys, fractional Chern numbers ($C = 1/2, 1/3, \ldots$) arise from Berry-curvature singularities near band. In particular, the least common multiple structure ($\mathrm{LCM}(6, 12, 8) = 24$) appearing in Berry-phase quantization of metallic bands closely mirrors the structure obtained from our hyperbolic geometry.

The Zak phase generalizes the Berry phase to 1D Brillouin zones and appears quantized in centrosymmetric metals and alloys:

$$\gamma = \oint_{\mathrm{BZ}} \mathbf{A}(\mathbf{k})\cdot d\mathbf{k} = n\pi, \qquad n \in \mathbb{Z}.$$

Quantized Zak phases have been measured directly [36] and shown to control polarization, edge modes, and transport anomalies. In 3D metals, similar quantized Berry windings govern Fermi-surface topology, including Weyl node charges and nodal-line drumhead states [37]. These winding numbers correspond to discrete geometric sectors of momentum space, providing a natural condensed-matter analogue of our $\pi/24$ hyperbolic sectorization.

Across the above examples, three recurring structural details appear. First, there is a discrete phase or winding number. Also, the electromagnetic response is quantized, typically in units proportional to e^2/h or α. A topological constraint, such as a symmetry, inversion, or modular invariance, restricts the set of allowed sectors.

This reflects our reconstruction of the vacuum impedance, in which a discrete geometric selector fixes the admissible (E, B) sectors, and the fine-structure constant emerges from a minimal discrete angle.

https://doi.org/10.3390/sym18020277

The appearance of rational, symmetry-protected electromagnetic phases in metals and alloys thus provides an independently established physical demonstration that discrete geometric sectorization is a measurable condensed-matter phenomenon. Our hyperbolic model can therefore be viewed as a continuum analogue of the Berry-phase sector structures realized in crystalline materials, suggesting that the $\pi/24$ partition may represent a universal discrete angle at the interface between electromagnetic geometry and topological matter.

5. Discussion

The appearance of the discrete angle $\pi/24$ in our construction suggests experimentally accessible consequences in systems where electromagnetic or structural response is governed by discrete rotational or modular symmetries. In quasicrystals and aperiodic 2D materials, $\mathrm{SL}(2,\mathbb{Z})$ modular symmetry organizes the allowed Fourier sectors of the reciprocal lattice [21]. Similarly, in topological phases of matter, phase winding and Berry curvature often concentrate in discrete angular sectors determined by crystalline or emergent rotational symmetry [2,4].

The appearance of a discrete sector angle does not vacuum field quantization. It is an experimentally meaningful statement only if the probe couples to a sectorized reciprocal-space structure. In crystalline and quasi-crystalline metals, discrete rotational order organizes reciprocal space into symmetry-related wedges, so that scattering intensities are naturally analyzed in angular sectors. Our $\pi/24$ hypothesis then predicts that responses built from mixed electric–magnetic channels are extremized when the measurement protocol (polarization/phase discretization) and the reciprocal-space sectorization share a common angular refinement. This can be tested by comparing angular-resolved scattering/response data under controlled polarization-phase stepping. A preferred refinement at $N = 24$ sectors would be a direct evidence of the proposed geometric sectorization.

Because $\pi/24$ is the least common sector compatible with the observed $\{\pi/6, \pi/12, \pi/8\}$ discretizations in interferometric and reciprocal-space settings, we predict that physical observables that depend on phase accumulation or EM duality should exhibit enhanced response at angular separations $\Delta\theta = \pi/24$. This includes the intensity distribution of GISAXS diffraction peaks [38].

A direct prediction of this framework is that scattering intensities, optical conductivities, or magneto-optical rotation angles should show extremal or resonant behavior at angular partitions corresponding to $\pi/24$. This reflect the geometric sector that also determines the electromagnetic constants in our construction. Observation of such $\pi/24$-enhanced sectors independent of microscopic details would strongly support the hypothesis that topological EM response is governed by a universal geometric partitioning of phase space. This connects condensed matter observables directly to the phase topology of the electromagnetic vacuum, providing a testable connection between solid-state symmetries and the proposed geometric foundation of Z_0 and α.

The geometric predictions discussed above can be tested through standard experimental probes of electromagnetic response in solid-state systems.

GISAXS and X-ray scattering measurements on metallic thin films reveal intensity patterns organized in angular sectors whose structure is a test platform with the $\pi/24$ partition underlying our hyperbolic selector [38]. This establishes a concrete link between the dimensionless phase geometry employed here and experimentally accessible symmetry patterns in metals and alloys.

Also, in thin films of topological materials, the predicted discretization of electric and magnetic channels can be probed via magneto-optical Kerr and Faraday rotation measurements [10]. Transport measurements in magnetic topological materials and anomalous Hall metals, Hall and longitudinal conductivities measured as functions of magnetic

field, film thickness, or strain also allow the test of discrete electromagnetic sectors. In plasmonic metallic thin films and simple metal alloys, the electromagnetic impedance and phase response can be accessed using terahertz time-domain spectroscopy or impedance-matched microwave resonators.

The proposed framework can be confronted with an experiment in materials where electromagnetic response coefficients are quantized or symmetry-protected. A promising platform is offered by magnetic topological materials and metallic thin films exhibiting anomalous Hall responses, such as Cr- or Mn-doped $(Bi,Sb)_2Te_3$ and $MnBi_2Te_4$. In these systems, electromagnetic transport coefficients are governed by Berry curvature and Chern numbers, producing quantized responses which are insensitive to microscopic details [39,40].

Also, plasmonic metallic thin films and simple metal alloys (e.g., Au, Ag, Al) provide an experimentally flexible environment in which electromagnetic phase and impedance can be measured with high precision [41].

While the present analysis is grounded in experimentally accessible solid-state systems, the underlying symmetry structures may plausibly persist across scales.

6. Summary and Conclusions

We have presented a geometric construction in which the electromagnetic vacuum is described through a Lorentz-invariant hyperbolic selector whose integer-square structure uniquely fixes the electric–magnetic partition. This selector determines the dimensionless part of the vacuum impedance, while the dimensional scale arises solely from quantum metrology through the von Klitzing constant. Thus the free-space impedance is not introduced as an axiom but reconstructed from symmetry and minimal discrete assumptions.

The same hyperbolic geometry leads to a natural normalization of the fine-structure constant via a universal sector angle $\pi/24$, derived from consistent discretizations of electromagnetic phase. This construction mirrors well-established mechanisms in metals and alloys, where discrete rotational symmetries, Berry phases, Zak phases, and Chern numbers enforce quantized electromagnetic responses. In this broader context, the $(6,5)$ selector behaves analogously to a topological invariant that encodes the allowed electromagnetic sectors.

Because the geometric selector and the discrete sector angle contain no tunable parameters, the framework makes experimentally testable predictions. Physical observables governed by angular phase accumulation, including GISAXS diffraction patterns, magneto-optical responses, and Berry phase controlled transport should display enhanced or extremal features at the universal sector angle $\pi/24$. Such behavior would indicate that the same discrete geometric structure responsible for quantized responses in metals and alloys also organizes the electromagnetic vacuum.

These results place the vacuum impedance, the fine-structure constant, and solid-state topological responses within a unified symmetry–geometric picture. This suggests that dimensionless electromagnetic constants reflect a deeper discrete hyperbolic structure, underlying both the continuum vacuum and topological matter.

The present analysis establishes a geometric reference framework formulated in vacuum electrodynamics and flat space–time, where Lorentz-invariant hyperbolic geometry provides a unambiguous environment for the electromagnetic degrees of freedom. In material systems, additional response functions and symmetry constraints modify this reference structure, but do not invalidate it. Rather, they encode departures from the vacuum geometry in a controlled and measurable way. In this sense, the vacuum construction serves as a baseline against which electromagnetic response in metals, thin films, and topological materials can be systematically interpreted.

https://doi.org/10.3390/sym18020277

In non-vacuum media, material-dependent permittivity, permeability, and topology are expected to deform the simple hyperbolic structure. In curved space–time the local Lorentz invariant may acquire geometric corrections. Nevertheless, the framework naturally suggests extensions toward bulk–boundary relations. Geometric constraints in the bulk determine boundary responses, in close analogy with holographically inspired constructions.

Finally, we emphasize that the purpose of this work is not to rederive or redefine fundamental constants. We wish to highlight recurring symmetry patterns that manifest clearly in metallic and solid-state systems. The fact that similar geometric structures appear compatible with more fundamental theoretical frameworks is presented here as an indication of structural continuity across scales. This is not a claim of unification. In this sense, metals and topological materials serve as experimentally controllable environment for probing symmetry principles that may extend beyond solid state physics.

Funding: This research received no external funding.

Data Availability Statement: The original contributions presented in this study are included in this article. Further inquiries can be directed to the corresponding author.

Acknowledgments: The author acknowledges useful discussions and informal exchanges with colleagues.

Conflicts of Interest: The author declares no conflicts of interest.

References

1. Thouless, D.J.; Kohmoto, M.; Nightingale, M.P.; den Nijs, M. Quantized Hall Conductance in a Two-Dimensional Periodic Potential. *Phys. Rev. Lett.* **1982**, *49*, 405. [CrossRef]
2. Hasan, M.Z.; Kane, C.L. Colloquium: Topological Insulators. *Rev. Mod. Phys.* **2010**, *82*, 3045. [CrossRef]
3. Qi, X.-L.; Zhang, S.-C. Topological Insulators and Superconductors. *Rev. Mod. Phys.* **2011**, *83*, 1057. [CrossRef]
4. Xiao, D.; Chang, M.-C.; Niu, Q. Berry Phase Effects on Electronic Properties. *Rev. Mod. Phys.* **2010**, *82*, 1959. [CrossRef]
5. Deser, S.; Teitelboim, C. Duality Transformations of Abelian and Non-Abelian Gauge Fields. *Phys. Rev. D* **1976**, *13*, 1592. [CrossRef]
6. Gaillard, M.K.; Zumino, B. Duality Rotations for Interacting Fields. *Nucl. Phys. B* **1981**, *193*, 221. [CrossRef]
7. Witten, E. On S-Duality in Abelian Gauge Theory. *Sel. Math.* **1995**, *1*, 383. [CrossRef]
8. von Klitzing, K. The Quantized Hall Effect. *Rev. Mod. Phys.* **1986**, *58*, 519–531. [CrossRef]
9. BIPM. *The International System of Units (SI)*, 9th ed.; Bureau International des Poids et Mesures: Sèvres, France, 2019.
10. Maciejko, J.; Qi, X.-L.; Drew, H.D.; Zhang, S.-C. Topological Quantization in Units of the Fine Structure Constant. *Phys. Rev. Lett.* **2010**, *105*, 166803. [CrossRef]
11. Essin, A.M.; Moore, J.E.; Vanderbilt, D. Magnetoelectric Polarizability and Axion Electrodynamics in Crystalline Insulators. *Phys. Rev. Lett.* **2009**, *102*, 146805. [CrossRef]
12. Qi, X.-L.; Hughes, T.L.; Zhang, S.-C. Topological Field Theory of Time-Reversal Invariant Insulators. *Phys. Rev. B* **2008**, *78*, 195424. [CrossRef]
13. Vazifeh, M.M.; Franz, M. Electromagnetic Response of Weyl Semimetals. *Phys. Rev. Lett.* **2013**, *111*, 027201. [CrossRef]
14. Deaver, B.S.; Fairbank, W.M. Experimental Evidence for Quantized Flux in Superconducting Cylinders. *Phys. Rev. Lett.* **1961**, *7*, 43. [CrossRef]
15. Doll, R.; Näbauer, M. Experimental Proof of Magnetic Flux Quantization. *Phys. Rev. Lett.* **1961**, *7*, 51. [CrossRef]
16. Tinkham, M. *Introduction to Superconductivity*, 2nd ed.; McGraw–Hill: Columbus, OH, USA, 1996.
17. Berry, M.V. Quantal Phase Factors Accompanying Adiabatic Changes. *Proc. R. Soc. A* **1984**, *392*, 45–57. [CrossRef]
18. Zak, J. Berry's Phase for Energy Bands in Solids. *Phys. Rev. Lett.* **1989**, *62*, 2747–2750. [CrossRef] [PubMed]
19. Armitage, N.P.; Mele, E.J.; Vishwanath, P. Weyl and Dirac Semimetals in Three-Dimensional Solids. *Rev. Mod. Phys.* **2018**, *90*, 015001. [CrossRef]
20. Haldane, F.D.M. Model for a Quantum Hall Effect without Landau Levels: Condensed-Matter Realization of the 'Parity Anomaly'. *Phys. Rev. Lett.* **1988**, *61*, 2015–2018. [CrossRef] [PubMed]
21. Mermin, N.D. The Space Groups of Two-Dimensional Quasicrystals. *Rev. Mod. Phys.* **1992**, *64*, 3. [CrossRef]
22. Nakahara, M. *Geometry, Topology and Physics*; IOP Publishing: Bristol, UK, 2003.
23. Frankel, T. *The Geometry of Physics*, 3rd ed.; Cambridge University Press: Cambridge, UK, 2011.
24. Shapere, A.; Wilczek, F. (Eds.) *Geometric Phases in Physics*; World Scientific: Singapore, 1989.
25. Katok, A.; Hasselblatt, B. *Introduction to the Modern Theory of Dynamical Systems*; Cambridge University Press: Cambridge, UK, 1995.

26. Silberstein, L. Elektromagnetische Grundgleichungen in bivectorieller Behandlung. *Ann. Phys.* **1907**, *327*, 579–586. [CrossRef]
27. Bialynicki-Birula, I. Electromagnetic field: Its quantization, coherent states, and Riemann–Silberstein representation. *Acta Phys. Pol. A* **1994**, *86*, 97.
28. Sommerfeld, A. Zur Quantentheorie der Spektrallinien. *Ann. Phys.* **1916**, *356*, 1–94. [CrossRef]
29. Schwinger, J. On Quantum-Electrodynamics and the Magnetic Moment of the Electron. *Phys. Rev.* **1948**, *73*, 416–417. [CrossRef]
30. Dyson, F.J. Fifty years of quantum electrodynamics. In *QED: The Strange Theory of Light and Matter*; Princeton University Press: Princeton, NJ, USA, 1990; pp. 1–45.
31. Workman, R.L.; Burkert, V.D.; Crede, V.; Klempt, E.; Thoma, U.; Tiator, L.; Agashe, K.; Aielli, G.; Allanach, B.; Amsler, C.; et al. Review of Particle Physics. *Prog. Theor. Exp. Phys.* **2022**, *2022*, 083C01. [CrossRef]
32. Gross, D.J.; Wilczek, F. Ultraviolet behavior of non-Abelian gauge theories. *Phys. Rev. Lett.* **1973**, *30*, 1343–1346. [CrossRef]
33. Li, R.; Wang, J.; Qi, X.-L.; Zhang, S.-C. Dynamical Axion Field in Topological Magnetic Insulators. *Nat. Phys.* **2010**, *6*, 284. [CrossRef]
34. Nagaosa, N.; Sinova, J.; Onoda, S.; MacDonald, A.H.; Ong, N.P. Anomalous Hall Effect. *Rev. Mod. Phys.* **2010**, *82*, 1539. [CrossRef]
35. Šmejkal, L.; Jungwirth, T.; Sinova, J. Topological Antiferromagnetic Spintronics. *Nat. Phys.* **2018**, *14*, 242. [CrossRef]
36. Atala, M.; Aidelsburger, M.; Barreiro, J.T.; Abanin, D.; Kitagawa, T.; Demler, E.; Bloch, I. 2Direct measurement of the Zak phase in topological Bloch bands. *Nat. Phys.* **2013**, *9*, 795–800. [CrossRef]
37. Fang, C.; Weng, H.; Dai, X.; Fang, Z. Topological nodal line semimetals. *Chin. Phys. B* **2016**, *25*, 117106. [CrossRef]
38. Renaud, G.; Lazzari, R.; Leroy, F. Probing surface and interface morphology with grazing incidence small angle X-ray scattering. *Surf. Sci. Rep.* **2009**, *64*, 255–380. [CrossRef]
39. Yu, R.; Zhang, W.; Zhang, H.-J.; Zhang, S.-C.; Dai, X.; Fang, Z. Quantized anomalous Hall effect in magnetic topological insulators. *Science* **2010**, *329*, 61–64. [CrossRef] [PubMed]
40. Chang, C.-Z.; Zhang, J.; Feng, X.; Shen, J.; Zhang, Z.; Guo, M.; Li, K.; Ou, Y.; Wei, P.; Wang, L.-L.; et al. Experimental observation of the quantum anomalous Hall effect. *Science* **2013**, *340*, 167–170. [CrossRef]
41. Gramotnev, D.K.; Bozhevolnyi, S.I. Plasmonics beyond the diffraction limit. *Nat. Photonics* **2010**, *4*, 83–91. [CrossRef]